

Electronic Supplementary Information for

**On the anomalous optical conductivity dispersion of electrically
conducting polymers: ultra-wide spectral range ellipsometry
combined with a Drude-Lorentz model**

Shangzhi Chen¹, Philipp Kühne², Vallery Stanishev², Sean Knight³, Robert Brooke⁴, Ioannis Petsagkourakis¹, Xavier Crispin¹, Mathias Schubert^{2,3,5}, Vanya Darakchieva^{2*}, Magnus P. Jonsson^{1*}

1 Laboratory of Organic Electronics, Department of Science and Technology (ITN), Linköping University, SE-601 74 Norrköping, Sweden

2 Terahertz Materials Analysis Center, Department of Physics, Chemistry and Biology (IFM), Linköping University, SE-581 83 Linköping, Sweden

3 Department of Electrical and Computer Engineering, University of Nebraska-Lincoln, Lincoln, Nebraska, 68588-0511, USA

4 RISE Acreo, SE-601 74 Norrköping, Sweden

5 Leibniz-Institut für Polymerforschung Dresden e.V., 01069 Dresden, Germany

* Corresponding author. E-mail: vanya.darakchieva@liu.se (V. D.), magnus.jonsson@liu.se (M.P.J.)

Ellipsometry fitting procedures

1. Procedure for the Drude-Lorentz model

Different spectral ranges can provide insights into various physical processes in the conducting polymers and the parameters for the whole model could be fitted or determined in either an individual spectral range or several connected ranges simultaneously. Some basic strategies are listed below.

Before the deposition of the PEDOT layer, the sapphire substrates were first measured and modelled with the anisotropic model reported in previous research by Schubert et al.¹ The model fits with experimental data quite well showing a thickness of 431 μm , which agrees with the complementary measurement by micrometer. A strong interference pattern can be observed with bare sapphire substrates (see **Figure S5**). The left panel presents raw data for the sapphire substrate and the right panel shows result for the polymer sample on sapphire. The sharp peaks from sapphire is hidden by the PEDOT layer in the right figure but the periodicity interference pattern remains. The pattern is related to Fabry-Perot interference and disappears for wavelengths approaching 40 μm , far less than the thickness of the substrate.'

In the UV-Vis-NIR range, the influence from mobile carriers on the optical conductivity and permittivity (σ_D and ϵ_D) is relatively small due to the fact that polymers have a low plasma frequency (around or below 1 eV)^{2,3} and possibly compensated for or covered by localization effects at low frequencies (see **Figure S1** and **S2**). Therefore, the Drude terms are to a large extent determined from the MIR range. Permittivity originating from interband transitions ϵ_{in} can be determined within the UV-Vis-NIR range while contributions from molecule vibrations ϵ_{vib} can be identified in the MIR and FIR ranges. The model obtained after completing the fitting from UV to FIR is used to compare with the experimental data in the THz range and observed differences between will be compensated for by the addition of one or several Lorentz oscillators. From this procedure we obtain the whole spectral range optical conductivity and permittivity for the material.

We first start with the UV-Vis-NIR region. This is the region containing interband transitions and the corresponding Lorentz oscillators obtained from the fit are listed in **Table S2**. The three identified interband transitions for the in-plane axis can be clearly associated to the peaks and shoulders shown in UV-Vis-NIR extinction spectrum of the thin film (see **Figure S9** (a)). The first oscillator located at 1.398 eV (the peak around 900 nm) can be attributed to the excitation transition from the HOMO level to the lower bipolaron band, implying a high conductivity, which is in agreement with previous literature.^{4,5} The second oscillator located at 2.224 eV (at about 560 nm) corresponds to the excitation transition from HOMO level to LUMO level of neutral or lightly-doped PEDOT.⁴ As expected for highly conducting doped PEDOT prepared by VPP, this resonator has small amplitude and large broadening and its features are not obvious in the extinction spectrum. The last oscillator centered at 6.564 eV (below 200 nm) can be correlated with absorption by the tosylate ions, as confirmed by other studies.^{5,6} The out-of-plane features can hardly be identified with a single absorption or reflection measurement due to its small thickness less than 200 nm. The thickness of VPP PEDOT:Tos samples is influenced by both ratio of the oxidant solution and the polymerization time and there is a limit for obtaining thicker films as those made by drop casting.^{2,4} Therefore, it is difficult to probe the out-of-plane information of the samples via the conventional optical characterization approaches that only rely on the intensity instead of polarization state of the light.

We now turn to the MIR and FIR range and first note that both ψ and Δ show smooth and relatively flat curves in the vibration-free region from around 0.25 to 0.8 eV (**Figure S6** (a) and (b) or **Figure 2** (c)). This region is therefore suitable for determining the initial Drude term parameters for both in-plane

and out-of-plane directions that could be used later for the final fitting of the whole spectral range. These parameters are shown in **Table 1**. While some studies in the MIR range treated PEDOT films as isotropic, we found that some detailed features, especially those between 0.08 eV and 0.2 eV (see **Figure 2 (c)**), could only be reproduced by an anisotropic model, with same charge density but different charge carrier mobility and phonon resonance modes for the in-plane and out-of-plane directions.^{7, 8} The resulting fit is excellent throughout the MIR and FIR range (see **Figure 2 (c)**).

We identified 36 in-plane (from UV to THz) and 14 out-of-plane Lorentz oscillators (from UV to MIR) and **Figure 4** present their specific contributions to the optical conductivity dispersion with their individual amplitude and broadening. Most of these Lorentz oscillators can be indexed to different vibrational resonance modes relating to the various stretching modes of chemical bonds in the VPP PEDOT:Tos, such as 1470-1500 cm^{-1} for C-C and C=C bonds stretching (0.18-0.19 eV), 840 cm^{-1} for C-S bonds vibration (around 0.10 eV), and 970 cm^{-1} for EDOT ring deformations (about 0.12 eV) as confirmed by FTIR (see **Figure S10 (b)**) and in agreement with those reported in literature.^{9, 10} Due to natural variations in the polymerization process, the detailed positions and broadening of the molecule vibrational modes may also vary a bit between samples.

We complete the fit and extend the range to the FIR and THz by including several additional Lorentz oscillators to account for non-Drude behavior (as also included in **Figure 4**). One Lorentz oscillator was added in the THz range to compensate for the difference between experimental data which the model for UV to FIR generated in THz range. This THz oscillator has a large amplitude and can improve the overall fitting quality for the THz range. Adding these Lorentz oscillators to the previous model gives us the final optical conductivity and permittivity model for the VPP PEDOT:Tos thin films (see **Figure 3**).

2. Procedure for the LMD model

The LMD model was used for VPP PEDOT:Tos thin films without including vibrational resonance modes. To improve the fitting quality in the UV-Vis-NIR region, interband transitions similar to those in the Drude-Lorentz model were added. A single fit was applied for the full spectral range and **Table 1** lists the parameters obtained for the minimal MSE case. The fittings at low frequencies (THz) are good, but there are large deviations in the MIR range, especially in the range from 0.2 eV to 0.8 eV. The permittivity dispersion curves from LMD model (blue curve in **Figure 3**) shows similar feature at low frequencies as the Drude-Lorentz model.

3. Procedure for the Drude-Smith model

Similar as for the LMD model, we account for interband transitions but not vibrations for the Drude-Smith model, and use a single fit for the full spectral range. Although the permittivity dispersion curve of the Drude-Smith model is similar to the other two models, the extracted parameters are quite different: both the charge carrier density and mobility are much larger compared with the electrically measured values (see **Table 1**).

The Drude-Smith model have been widely used to interpret measurement results from THz-TDS measurements for the range from 0.3 to 3 THz.¹¹⁻¹³ We therefore also applied this model to this limited spectral range for our ellipsometric data. The fitted curves and the extracted data are displayed in **Figure S7** and **Table 1**, respectively, denoted as DS-THz. The values are comparable to those reported in literature, with overestimated charge mobility and underestimated charge density.^{11, 12} The large discrepancy between the parameters predicted (obtained) from the Drude-Lorentz model (electrical

measurements) and the DS-THz model implies that the model fitting for the narrow spectral range would be inaccurate and unreliable since more than one set of reasonable parameters could be obtained with minimal MSE. Regarding this, optical measurements as well as model fitting in an ultra-wide spectral range would be one the most reliable ways to determine materials' properties with high precision and accuracy.

Supporting Tables and Figures

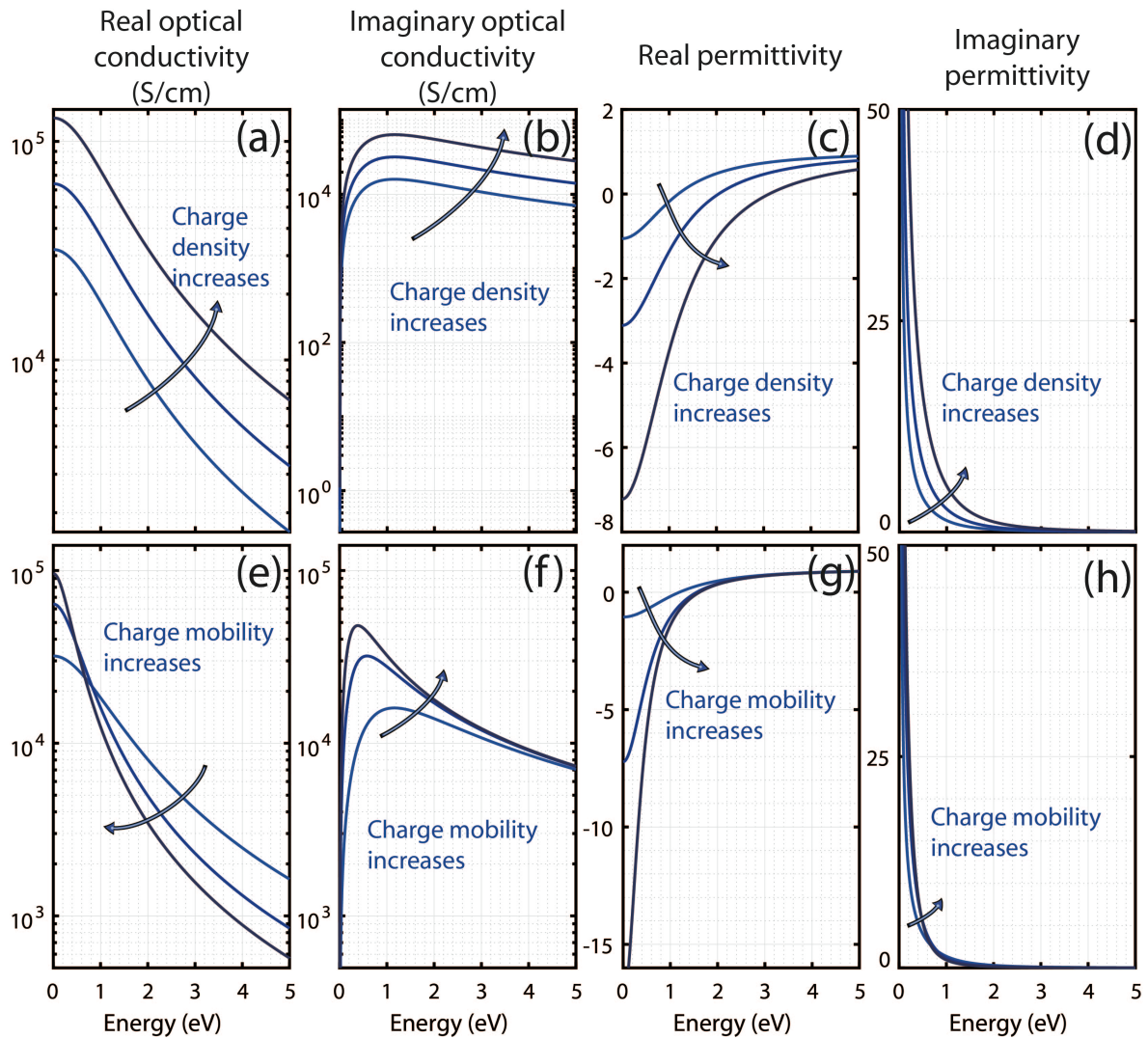


Figure S1. Examples of optical conductivity and permittivity dispersion curves of the Drude model. (a), (b), (c), and (d) show the influence of charge density change on optical conductivity and permittivity. (e), (f), (g), and (h) demonstrate the effect of charge mobility variation on optical conductivity and permittivity. For illustration, the free carrier density is $2 \times 10^{21} \text{ cm}^{-3}$ (or $4 \times 10^{21} \text{ cm}^{-3}$ or $8 \times 10^{21} \text{ cm}^{-3}$), and the mobility is $1 \text{ cm}^2/\text{Vs}$ (or $2 \text{ cm}^2/\text{Vs}$ or $3 \text{ cm}^2/\text{Vs}$). The effective mass is assumed 1.

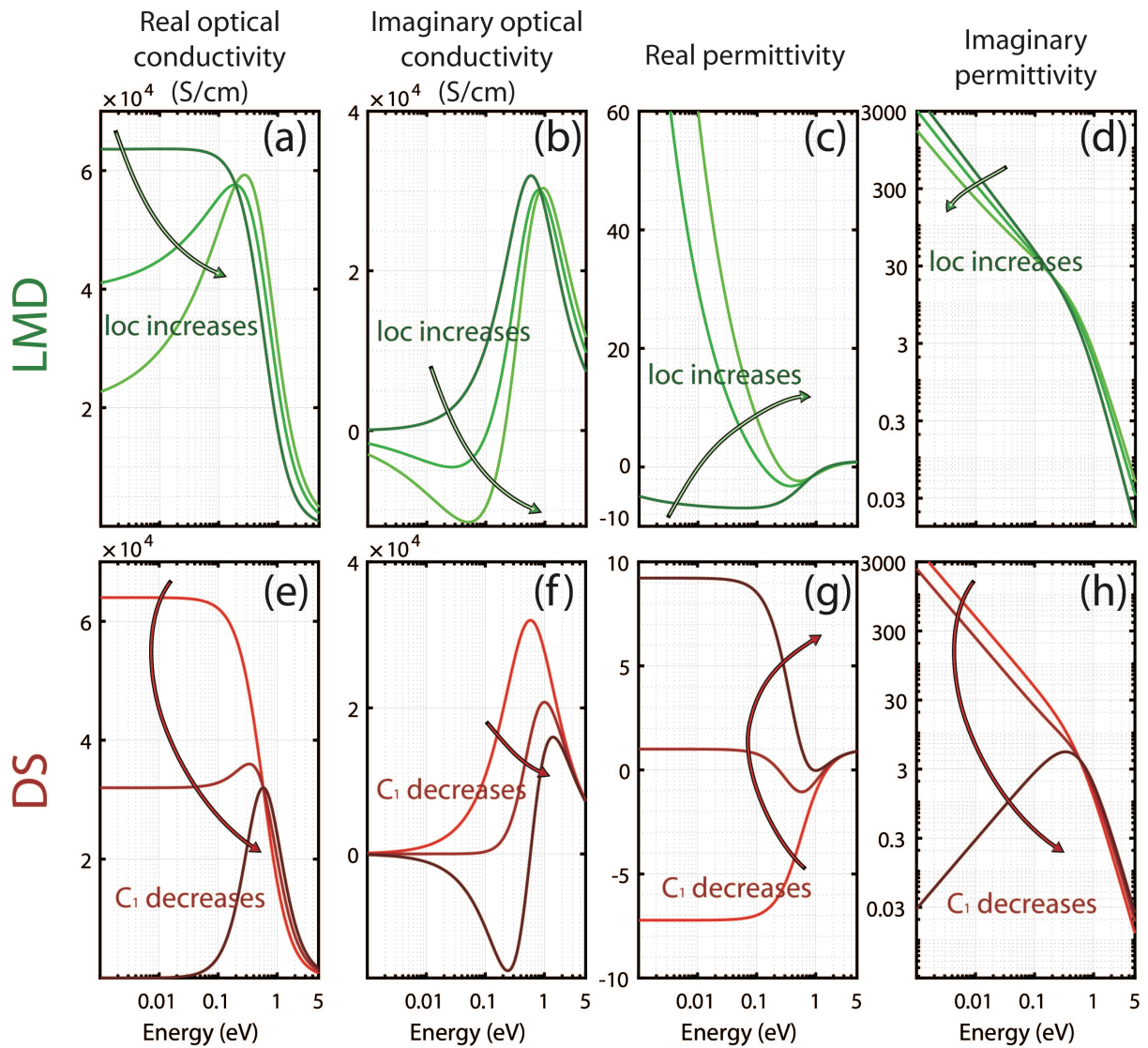


Figure S2. Examples of optical conductivity and permittivity dispersion curves of the LMD model (a, b, c, d) and of the Drude-Smith (DS) model (e, f, g, h). Tuning the modification parameters (*loc* or C_1) affects the curve shape of the models, as indicated by the green arrow (LMD) and the red arrow (red). The free carrier density is $2 \times 10^{21} \text{ cm}^{-3}$ and the mobility is $2 \text{ cm}^2/\text{Vs}$. *loc* values can be 9×10^{-31} (light green), 5×10^{-31} (green), and 9×10^{-33} (dark green). C_1 values can be 0 (light red), -0.5 (red), and -1 (dark red). The modification term in the LMD model or the DS model can produce an additional peak in MIR range for the optical conductivity and a dip feature at similar position for the real permittivity. For the LMD model, the real permittivity will reach positive infinity at zero frequency while for the Drude-Smith model, the DC permittivity is a finite value.

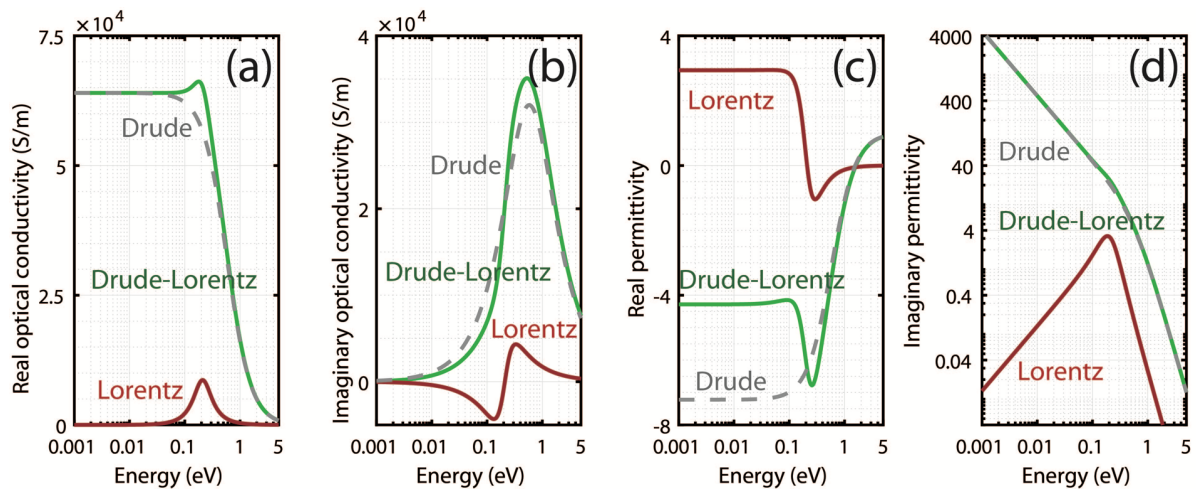


Figure S3. Illustration of the Drude-Lorentz model with only one Lorentz oscillator, at about 0.2 eV. (a and b) Example of optical conductivity provided by the Drude-Lorentz model (green solid line) together with the Drude contribution (grey dashed line) and the Lorentz oscillator contribution (red solid line). (c and d) Same as in (a and b), but for the corresponding permittivity.

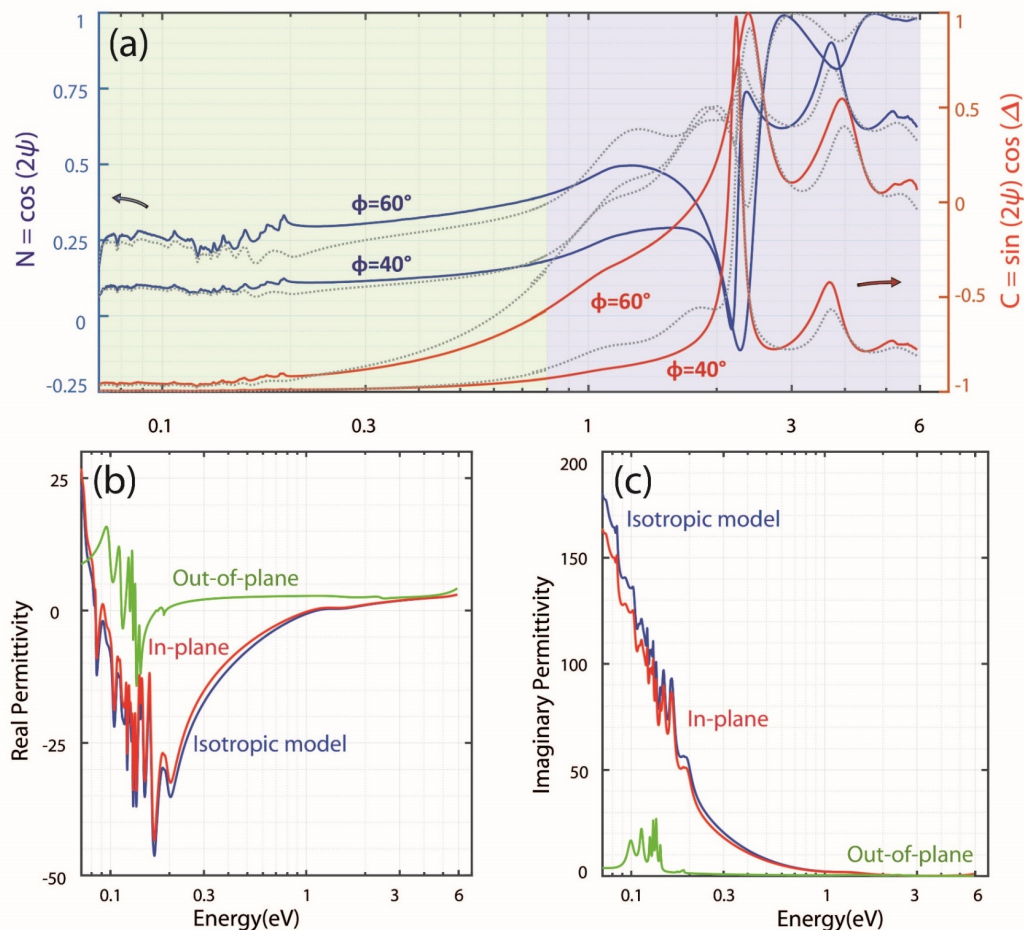


Figure S4. (a) Ellipsometry data (blue and red lines) of N and C for a VPP PEDOT:Tos thin film. The gray dotted lines are generated by the best-match Drude-Lorentz model using an optically isotropic structure. For the data presentation, only the UV-Vis-NIR and MIR range are used. (b) The real and (c) imaginary parts of the permittivity obtained from the isotropic model (blue lines) compared with the in-plane (red lines) and out-of-plane permittivity (green lines) from the uniaxial anisotropic model.

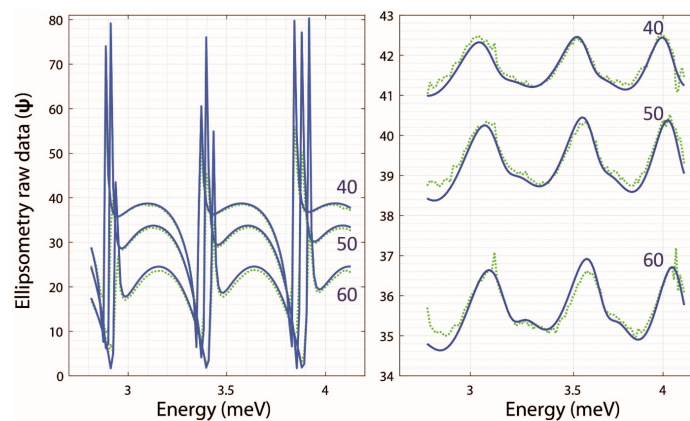


Figure S5. Ellipsometry raw data (ψ) for a bare sapphire substrate (left panel) and for PEDOT:Tos on this sapphire substrate (right panel). The thickness of the substrate is in the same range of the probe light (3 meV corresponds to about 413 μm), explaining the periodic pattern as Fabry-Perot interferences.

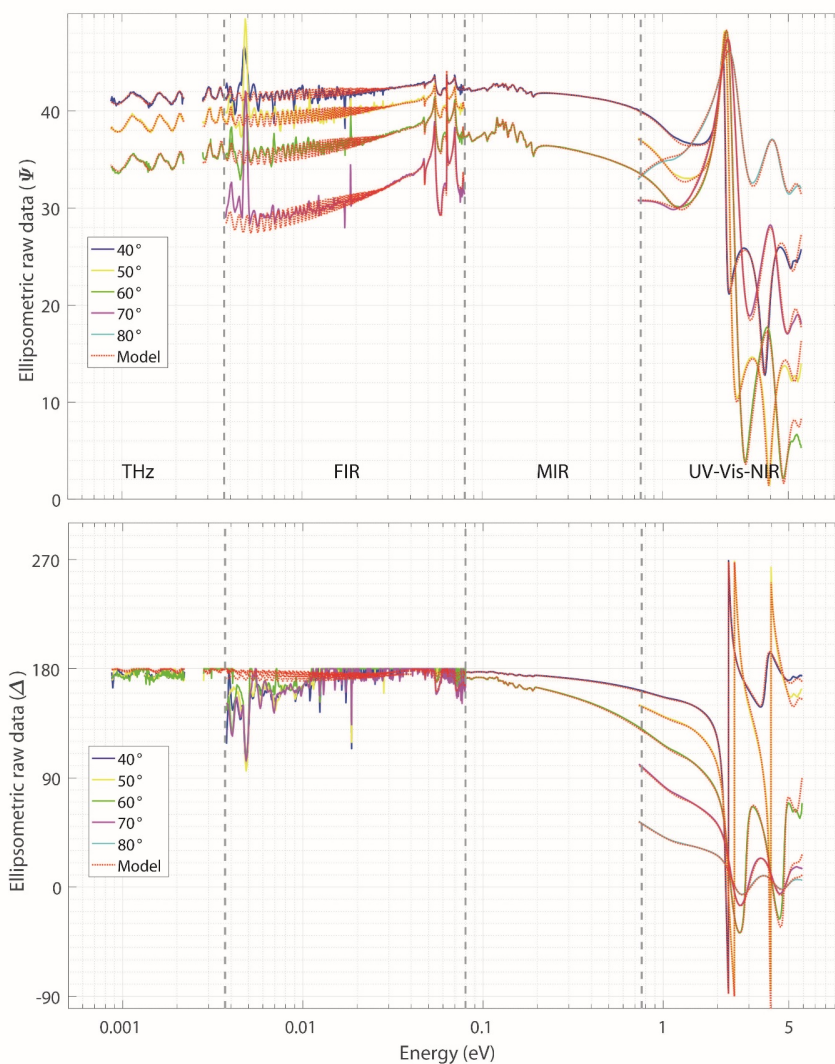


Figure S6. Ellipsometry raw data (a) ψ (top panel) and (b) Δ (bottom panel) of VPP PEDOT:Tos thin film sample for experimental (solid line) and the Drude-Lorentz model generated data (dashed line). The measurement covers four different spectral range and multiple incident angles were used.

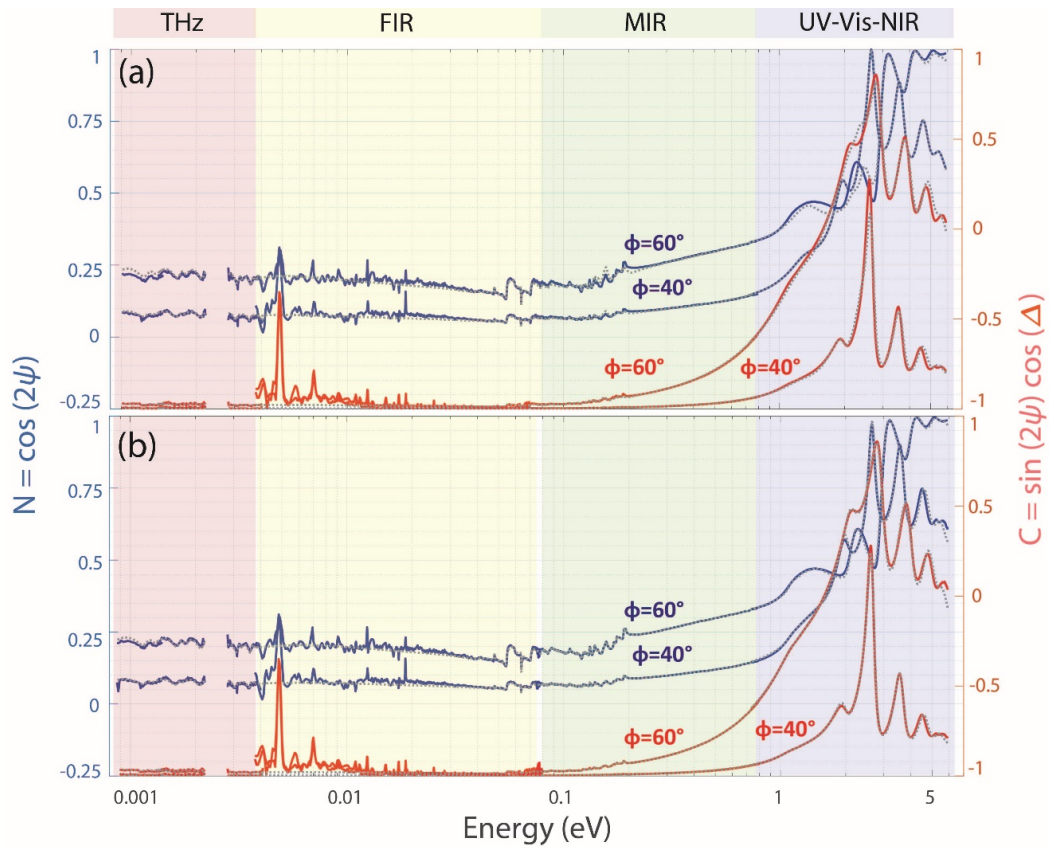


Figure S7. Ellipsometric raw data $N = \cos(2\psi)$ (blue) and $C = \sin(2\psi)\cos(\Delta)$ (red) and fitted curves (grey dotted lines) for a PEDOT:Tos thin film with a larger thickness (around 310 nm). In (a), the experimental results were fitted to the Drude-Lorentz model with same vibrational and interband oscillators as employed for the thin sample in Figure 2 (gray dotted lines). Four spectral ranges and multiple incident angles were employed. Except for some small deviations in the MIR range (around 0.2 eV) and visible range (around 1.5 eV), the model demonstrates its suitability for application for different PEDOT:Tos samples. Small deviations in the MIR range may be caused by differences in localization effects or vibrational resonances between the different samples. In (b), we have adjusted the parameters of several oscillators in order to account for small variations in material properties between samples, resulting in excellent fits to the experimental data.

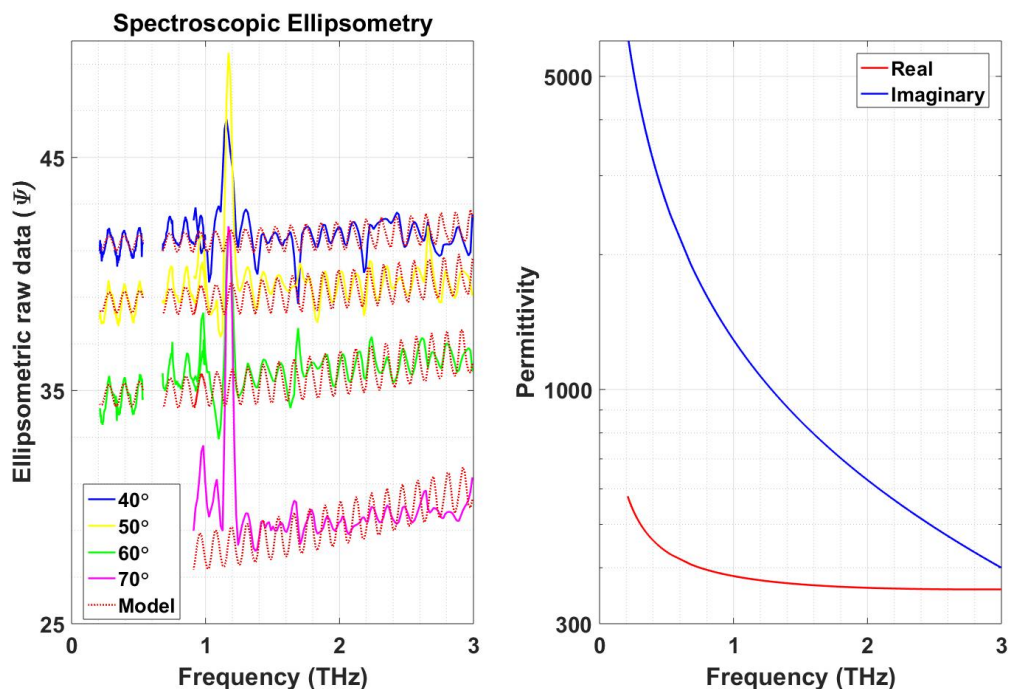


Figure S8. Experimental and model generated curves based on the Drude-Smith model in the spectral range from 0.3 THz to 3 THz (left panel), and the real and imaginary permittivity dispersion of the Drude-Smith model in this range (right panel). The film was considered isotropic and no interband transitions or phonon resonance modes were included.

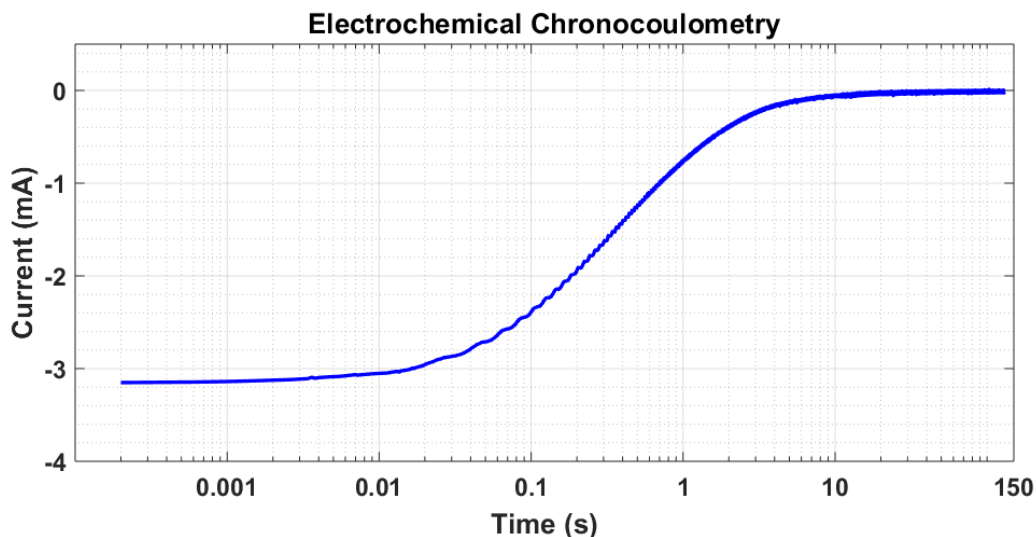


Figure S9. Electrochemical chronocoulometry for the de-doping process of a PEDOT:Tos film. The accumulated charge from the electrolyte compensated the charge carriers in the film to make it approach electrically neutral state. The integral of the current over time gives an estimate of the total amount of charge carriers of the film. In the case shown above, the accumulated charge is 5.15 mA·s (5.15×10^{-3} C) for the film with an area of 0.75 cm^2 and a thickness of 190 nm, thus giving a charge density of $2.26 \times 10^{21} \text{ cm}^{-3}$. Measurements on multiple samples provided an average charge density of $2.13 \times 10^{21} \text{ cm}^{-3}$.

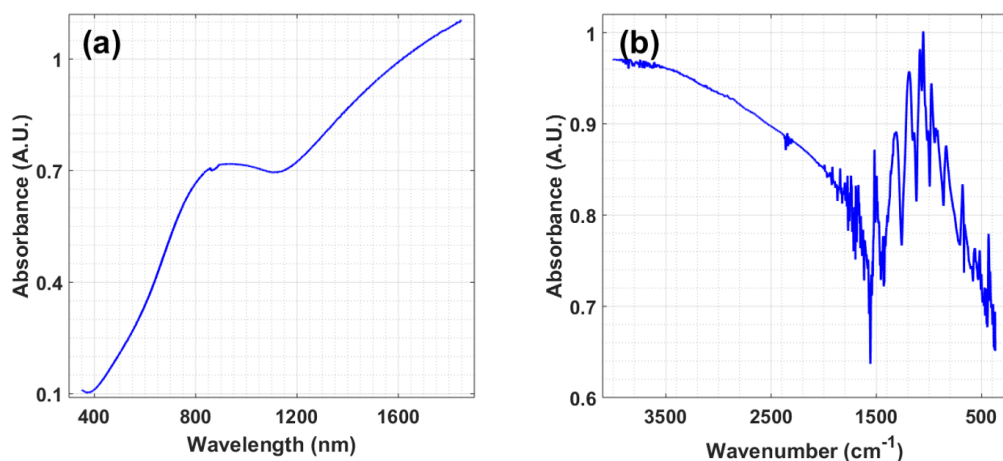


Figure S10. (a) UV-Vis-NIR absorption spectra and (b) FTIR spectra for a PEDOT:Tos thin film sample.

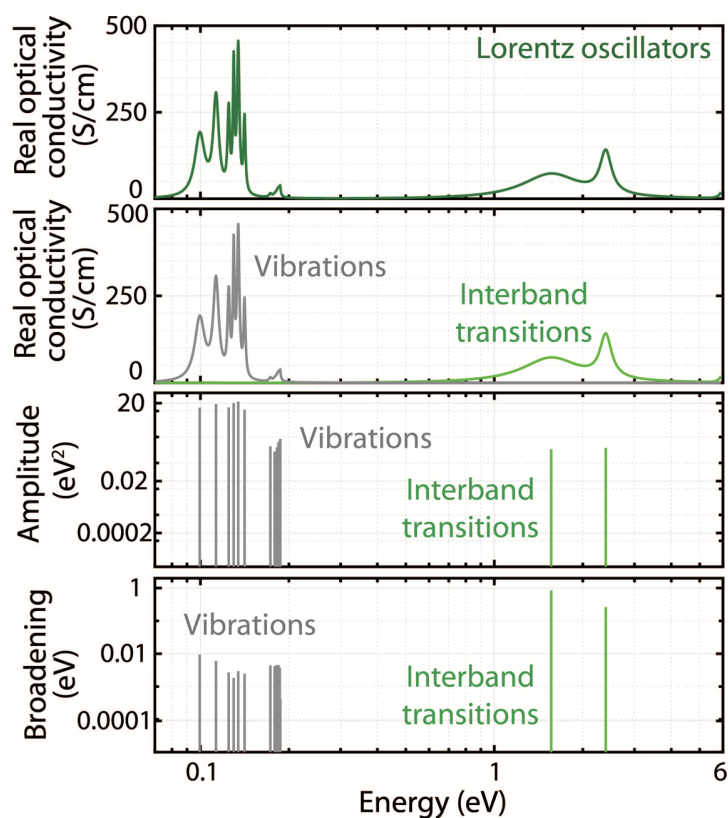


Figure S11. (a) Out-of-plane real optical conductivity dispersion of PEDOT:Tos thin film represented by multiple Lorentz oscillators (no Drude contribution is included) derived from Drude-Lorentz model. (b) The contributions to the real optical conductivity from interband transitions (green) and molecule vibrations (grey) are indicated. (c) and (d) display the amplitude and broadening parameters for each Lorentz oscillator. The parameters for these Lorentz oscillators are listed in Table S2.

Table S1. Electrical properties of PEDOT-based materials reported in the literature. Both in-plane and out-of-plane directions are included. It should be noted that some of the reported results were based on free-standing thick films (thickness larger than 10 μm), which are different from our VPP PEDOT:Tos thin films where the out-of-plane properties are difficult to characterize electrically.

Materials	In-plane transport			Out-of-plane transport			Ratio	Ref
	Mobility (cm^2/Vs)	Density (10^{21}cm^{-3})	Conductivity (S/cm)	Mobility (cm^2/Vs)	Density (10^{21}cm^{-3})	Conductivity (S/cm)		
PEDOT:Tos	1.6	2.6	790					14
PEDOT:PSS			300			0.1	300	15
PEDOT:PSS ¹			1×10^{-3}			2×10^{-6}	500	16
PEDOT:PSS			1×10^{-2}			4×10^{-4}	25	17
PEDOT:PSS			820			36	23	18
PEDOT:PSS	1.7	3.1	830					19
This work	2	2.2	700	0.09	2.2	32	22	

Table S2. The fitting parameters (amplitude, broadening, and characteristic frequency (energy)) for all the Lorentz oscillators in the ultra-wide spectral range ellipsometry model. Three sets of oscillators are indicated: in-plane, out-of-plane, and common oscillators. These data are also displayed in **Figure 4** and **Figure S11**.

	Amplitude (eV^2)	Energy (eV)	Broadening (eV)
In-plane Lorentz Oscillators	2.0101	6.5643	1.2289
	0.0513	2.2241	1.0018
	1.0455	1.3980	0.7602
	8.7831	0.1950	0.0229
	6.0144	0.1912	0.0399
	4.4142	0.1672	0.0061
	33.4820	0.1623	0.0094
	7.1438	0.1595	0.0028
	31.5740	0.1470	0.0074
	5.0272	0.1311	0.0062
	18.8160	0.1273	0.0036
	18.5430	0.1210	0.0019
	19.7350	0.1175	0.0090
	9.4388	0.1093	0.0045
	20.2150	0.1029	0.0061
	18.9170	0.0938	0.0112
	25.2510	0.0907	0.2395
	13.3290	0.0843	0.0018
	5.3172	0.0820	0.0032
	32.7570	0.0801	0.0187
11.6853	0.0740	0.0056	
17.4102	0.0703	0.0050	
32.0027	0.0531	0.0062	
11.0121	0.0492	0.0204	

¹ The PEDOT:PSS samples with low conductivities were purchased directly from the company without any further treatment (no secondary doping with DMSO, etc.). Various treatments including thermal, solvent, or vapor-assisted methods, can affect the conductivity of PEDOT-based materials by more than four orders of magnitude.

	18.8020	0.0380	0.0123
	45.9610	0.0321	0.1029
	265.8232	0.0035	0.0012
Out-of-plane Lorentz Oscillators	0.3786	2.3950	0.2632
	0.3382	1.5616	0.8558
	0.8452	0.1870	0.0004
Common Lorentz Oscillators shared by both directions	0.7190	0.1862	0.0038
	0.6233	0.1843	0.0045
	0.4008	0.1821	0.0047
	0.2741	0.1789	0.0042
	0.4364	0.1731	0.0044
	11.2760	0.1413	0.0025
	23.2541	0.1345	0.0029
	20.4612	0.1298	0.0018
	13.6841	0.1248	0.0027
	18.4170	0.1130	0.0060
	13.4221	0.0995	0.0094

References

1. M. Schubert, T. Tiwald and C. Herzinger, *Physical Review B* **61** (12), 8187 (2000).
2. N. Kim, B. H. Lee, D. Choi, G. Kim, H. Kim, J.-R. Kim, J. Lee, Y. H. Kahng and K. Lee, *Physical review letters* **109** (10), 106405 (2012).
3. K. Lee and A. J. Heeger, *Synthetic metals* **84** (1-3), 715-718 (1997).
4. J. Edberg, D. Iandolo, R. Brooke, X. Liu, C. Musumeci, J. W. Andreasen, D. T. Simon, D. Evans, I. Engquist and M. Berggren, *Advanced Functional Materials* **26** (38), 6950-6960 (2016).
5. O. Bubnova, Z. U. Khan, A. Malti, S. Braun, M. Fahlman, M. Berggren and X. Crispin, *Nature materials* **10** (6), 429 (2011).
6. J. Wang, K. Cai and S. Shen, *Organic Electronics* **15** (11), 3087-3095 (2014).
7. M. Schubert, C. Bundesmann, H. v. Wenckstern, G. Jakopic, A. Haase, N. K. Persson, F. Zhang, H. Arwin and O. Inganäs, *Applied physics letters* **84** (8), 1311-1313 (2004).
8. M. Schubert, C. Bundesmann, G. Jakopic, H. Maresch, H. Arwin, N. C. Persson, F. Zhang and O. Inganäs, *Thin Solid Films* **455**, 295-300 (2004).
9. H. Wang, H. Zhou, A. Gestos, J. Fang, H. Niu, J. Ding and T. Lin, *Soft Matter* **9** (1), 277-282 (2013).
10. J. Rodríguez-Moreno, E. Navarrete-Astorga, E. A. Dalchiele, R. Schrebler, J. R. Ramos-Barrado and F. Martín, *Chemical Communications* **50** (42), 5652-5655 (2014).
11. Y. Du, X. Cui, L. Li, H. Tian, W. X. Yu and Z. X. Zhou, *physica status solidi (b)* (2017).
12. F. Yan, E. P. J. Parrott, B. S. Y. Ung and E. Pickwell-MacPherson, *The Journal of Physical Chemistry C* **119** (12), 6813-6818 (2015).
13. M. Yamashita, C. Otani, M. Shimizu and H. Okuzaki, *Applied Physics Letters* **99** (14), 213 (2011).
14. S. Rudd, J. F. Franco - Gonzalez, S. Kumar Singh, Z. Ullah Khan, X. Crispin, J. W. Andreasen, I. Zozoulenko and D. Evans, *Journal of Polymer Science Part B: Polymer Physics* **56** (1), 97-104 (2018).
15. K. van de Ruit, I. Katsouras, D. Bollen, T. van Mol, R. A. J. Janssen, D. M. de Leeuw and M. Kemerink, *Advanced Functional Materials* **23** (46), 5787-5793 (2013).

16. A. M. Nardes, M. Kemerink, R. A. J. Janssen, J. A. M. Bastiaansen, N. M. M. Kiggen, B. M. W. Langeveld, A. J. J. M. Van Breemen and M. M. De Kok, *Advanced Materials* **19** (9), 1196-1200 (2007).
17. S.-I. Na, G. Wang, S.-S. Kim, T.-W. Kim, S.-H. Oh, B.-K. Yu, T. Lee and D.-Y. Kim, *Journal of Materials Chemistry* **19** (47), 9045-9053 (2009).
18. Q. Wei, M. Mukaida, K. Kiriwara and T. Ishida, *ACS Macro Letters* **3** (9), 948-952 (2014).
19. Q. Wei, M. Mukaida, Y. Naitoh and T. Ishida, *Advanced materials* **25** (20), 2831-2836 (2013).